

Anisotropy of the cosmic gamma-ray background from dark matter annihilation

Shin'ichiro Ando*

Department of Physics, School of Science, University of Tokyo, Tokyo 113-0033, Japan

Eiichiro Komatsu†

Department of Astronomy, University of Texas at Austin, Austin, TX 78712

(Dated: December 8, 2005; accepted January 13, 2006)

High-energy photons from pair annihilation of dark matter particles contribute to the cosmic gamma-ray background (CGB) observed in a wide energy range. Since dark matter particles are weakly interacting, annihilation can happen only in high density regions such as dark matter halos. The precise shape of the energy spectrum of CGB depends on the nature of dark matter particles — their mass and annihilation cross section, as well as the cosmological evolution of dark matter halos. In order to discriminate between the signals from dark matter annihilation and other astrophysical sources, however, the information from the energy spectrum of CGB may not be sufficient. We show that dark matter annihilation not only contributes to the mean CGB intensity, but also produces a characteristic *anisotropy*, which provides a powerful tool for testing the origins of the observed CGB. We develop the formalism based on a halo model approach to analytically calculate the three-dimensional power spectrum of dark matter clumping, which determines the power spectrum of annihilation signals. We show that the expected sensitivity of future gamma-ray detectors such as the Gamma Ray Large Area Space Telescope (GLAST) should allow us to measure the angular power spectrum of CGB anisotropy, if dark matter particles are supersymmetric neutralinos and they account for most of the observed mean intensity of CGB in GeV region. On the other hand, if dark matter has a relatively small mass, on the order of 20 MeV, and accounts for most of the CGB in MeV region, then the future Advanced Compton Telescope (ACT) should be able to measure the angular power spectrum in MeV region. As the intensity of photons from annihilation is proportional to the density squared, we show that the predicted shape of the angular power spectrum of gamma rays from dark matter annihilation is different from that due to other astrophysical sources such as blazars and supernovae, whose intensity is linearly proportional to density. Therefore, the angular power spectrum of the CGB provides a “smoking-gun” signature of gamma rays from dark matter annihilation. While the mean CGB intensity expected from dark matter halos with smooth density profiles is smaller than observed, the dark matter substructure within halos may provide the origin of additional “boost” factors for the annihilation signal. Our formalism can be used for any other radiation processes that involve collision of particles.

PACS numbers: 95.35.+d; 95.85.Pw; 98.70.Vc

I. INTRODUCTION

The energy density of the universe is dominated by invisible components: dark matter and dark energy, both of which are of unknown origin. Remarkable progress in both the theoretical and observational studies of the cosmic microwave background (CMB) anisotropy, Type Ia supernovae, and large-scale structure has allowed us to precisely determine what fraction of the total energy these dark components convey, $\Omega_\chi = 0.23$ and $\Omega_\Lambda = 0.73$ [1], where the subscripts χ and Λ denote dark matter particles and dark energy, respectively.

While the nature of dark energy is a complete mystery, there are several candidates for dark matter particles. Of which, the most popular candidate is the stable supersymmetric neutralino with mass on the order of GeV to TeV, which can explain the observed dark matter mass

density today. Although very weak, it is expected that dark matter particles may interact with the usual matter via scattering, interact with themselves, and/or annihilate into gamma rays, positrons, and neutrinos. The direct detection of particle dark matter is, therefore, under intensive and extensive efforts of both physicists and astronomers [2, 3, 4].

High-energy photons from annihilation of dark matter particles provide indirect means to probe the properties of dark matter. Annihilation signatures, especially gamma rays, have been searched for in regions where the dark matter density is expected to be high, as annihilation rate is proportional to the density squared, ρ_χ^2 . An obvious site is the central region of our Galaxy. Strong gamma-ray emission has been detected toward the Galactic center over a wide energy range, and the nature and origin of this emission have been investigated by many researchers [5, 6, 7, 8, 9, 10, 11, 12, 13]. Although both the spectrum and angular distribution of gamma rays from the Galactic center are well observed, it is still quite difficult to distinguish a dark matter component from the other possibilities such as emission from “ordinary” astrophysical objects; even future gamma-ray detectors and

*Electronic address: ando@utap.phys.s.u-tokyo.ac.jp

†Electronic address: komatsu@astro.as.utexas.edu

telescopes do not have sufficient resolution to remove all the other sources from the Galactic central image.

Another possibility is the extragalactic background light, the cosmic gamma-ray background (CGB), which has been measured in a wide energy range [14, 15, 16, 17, 18]. It has been speculated that some fraction of the CGB may originate from annihilation of dark matter particles in halos distributed over cosmological distances [19, 20, 21, 22, 23, 24, 25, 26, 27]. The dark matter contribution to the CGB depends on the nature of dark matter particles, such as their mass and annihilation cross section, as well as the cosmological evolution of dark matter halos. While it is likely that the dominant part of the CGB spectrum in the GeV region, detected by the Energetic Gamma Ray Experiment Telescope (EGRET) [14, 15], comes from unresolved blazars, i.e., beamed population of Active Galactic Nuclei (AGN), annihilating dark matter might give large contribution at some specific energy range.¹ Possible candidates for this case include the supersymmetric neutralino, as well as the Kaluza-Klein dark matter predicted by theories of universal extra-dimension (e.g., [4]) and heavy relic neutrinos [29, 30]. On the other hand, the origin of the CGB in MeV region is much less understood than in GeV region. The soft gamma-ray spectrum in 1–20 MeV cannot fully be attributed to either AGN or Type Ia supernovae or a combination of the two [31, 32]; thus, annihilation of dark matter particles is one of the most viable explanations for the CGB in MeV region, provided that the dark matter mass is around 20 MeV [26, 27]. Such a light dark matter particle was originally introduced to explain the origin of the 511 keV emission line from the Galactic center [33, 34], detected by the International Gamma-Ray Astrophysics Laboratory (INTEGRAL) [35, 36], which is otherwise difficult to explain. Therefore, the MeV dark matter is an attractive candidate that satisfies the observational constraints from both the Galactic center and the CGB,² while its particle physics motivation is less clear than for the neutralinos.

Dark matter annihilation may be a viable explanation for the CGB, but how do we know for sure that the CGB does come from annihilation? What would be a smoking-

gun signature for the annihilation signal? We argue that *anisotropy* of the CGB may provide a smoking-gun signature. Although the CGB is isotropic at the leading order, anisotropy should also exist if the CGB originates from cosmological halos. The future gamma-ray detectors with an enhanced sensitivity and angular resolution, such as the Gamma Ray Large Area Space Telescope (GLAST) or the Advanced Compton Telescope (ACT), should be able to see such anisotropy. We believe that the CGB anisotropy is going to be the key to discriminating between the dark matter annihilation signal and the other sources.

In this paper, we develop the formalism to analytically calculate the angular power spectrum of the CGB from dark matter annihilation. We calculate the angular power spectrum in GeV region (for supersymmetric neutralinos) as well as in MeV region (for MeV dark matter). We then discuss the detectability of CGB anisotropy in GeV region by GLAST and in MeV region by ACT, showing that the predicted anisotropy can be easily measured by 1-year operation of these experiments. The formalism given in this paper can also be used to evaluate the CGB anisotropy due to the other astrophysical objects with some modification. Note that the case of Type Ia supernovae has been discussed in Ref. [38], being complementary to the present study.

This paper is organized as follows. In Sec. II, we review the mean intensity of the CGB from dark matter annihilation. In Sec. III, we develop the formalism to calculate the power spectrum of CGB anisotropy in the context of the halo models. Results of the angular power spectrum are then shown in Sec. IV for both the neutralino and MeV dark matter. We compare the predictions with the expected sensitivities of the future gamma-ray detectors. In Sec. V, we discuss energy dependence of the obtained anisotropy (Sec. V A), other astrophysical sources which might contaminate the cosmological CGB (Sec. V B), and the effects of dark matter substructures (Sec. V C). In Sec. VI, we conclude the present paper with a brief summary.

II. COSMIC GAMMA-RAY BACKGROUND: ISOTROPIC COMPONENT

Since the gamma-ray emissivity from dark matter annihilation is proportional to the density squared, ρ_χ^2 , the CGB intensity (the number of photons per unit area, time, solid angle, and energy range) toward the direction \hat{n} can be generally expressed as

$$I_\gamma(\hat{n}, E_\gamma) = \int dr \delta^2(r, \hat{n}r) W([1+z]E_\gamma, r), \quad (1)$$

where E_γ is the observed gamma-ray energy, z is the redshift, r is the comoving distance out to an object at z , W is some function of gamma-ray energy and r that is given below, and δ is the overdensity at $\hat{n}r$ compared

¹ As has been known and is shown below, with the canonical choice of relevant parameters, dark matter annihilation cannot give enough contribution to the mean CGB intensity; one still needs large boost by some mechanism. In addition, its contribution is strongly constrained by gamma-ray observations toward the Galactic center [24]. However, one might avoid these constraints by invoking gamma-ray emission from sub-halos having $M \sim 10^{-6} M_\odot$ within host halos [25], or from density cusps forming around intermediate-mass black holes [28].

² After this paper has been submitted, Ref. [37] has appeared on the preprint server. They claim that the mass of MeV dark matter should be less than 3 MeV from a more accurate treatment of relativistic positrons annihilating with electrons in the interstellar medium. While we use $m_\chi = 20$ MeV throughout this paper, one can easily extend our calculations to arbitrary dark matter masses.

to the average dark matter mass density, $\bar{\rho}_\chi$, given by

$$\delta \equiv \frac{\rho_\chi}{\bar{\rho}_\chi}. \quad (2)$$

Because the dominant contribution comes from the dark matter halos, δ is always much larger than unity. Note that we label time by r (or redshift z used interchangeably), and space by $\mathbf{r} = \hat{\mathbf{n}}r$.

We first derive the specific form of the function W . The general formula for the intensity is given by [39]

$$E_\gamma I_\gamma(\hat{\mathbf{n}}, E_\gamma) = \frac{c}{4\pi} \int dz \frac{P_\gamma([1+z]E_\gamma, z, \hat{\mathbf{n}}r)}{H(z)(1+z)^4} \times e^{-\tau([1+z]E_\gamma, z)}, \quad (3)$$

where P_γ is the volume emissivity (energy of photons per unit volume, time, and energy range), $H^2(z) \equiv H_0^2[\Omega_m(1+z)^3 + \Omega_\Lambda]$ is the Hubble function in a flat universe, and we assume the standard values for cosmological parameters, $H_0 = 100 h \text{ km s}^{-1} \text{ Mpc}^{-1}$ with $h = 0.71$, $\Omega_m = 0.27$, and $\Omega_\Lambda = 0.73$. By the exponential factor, we incorporate the effect of the gamma-ray absorption due to pair creation with the diffuse extragalactic background light in the infrared or optical bands [40]; however, this effect is actually negligible for the cases we consider here where the gamma-ray energy is smaller than 1 TeV. The annihilation rate per unit volume is given by $(\rho_\chi/m_\chi)^2 \langle \sigma v \rangle / 2$, where m_χ is the mass of dark matter particle and $\langle \sigma v \rangle$ is the annihilation cross section times relative velocity averaged with the weight of the velocity distribution. The volume emissivity is therefore given by

$$P_\gamma(E_\gamma, z, \hat{\mathbf{n}}r) = E_\gamma \frac{dN_\gamma}{dE_\gamma} \frac{\langle \sigma v \rangle}{2} \left[\frac{\rho_\chi(z, \hat{\mathbf{n}}r)}{m_\chi} \right]^2, \quad (4)$$

where dN_γ/dE_γ is the gamma-ray spectrum per annihilation. Comparing Eq. (1) with Eqs. (3) and (4), and recalling that $dr = -cdz/H(z)$ and $\rho_\chi(z, \hat{\mathbf{n}}r) = \bar{\rho}_\chi(z)\delta(z, \hat{\mathbf{n}}r) = \Omega_\chi \rho_c(1+z)^3 \delta(z, \hat{\mathbf{n}}r)$, we obtain W as

$$W(E_\gamma, z) = \frac{\langle \sigma v \rangle}{8\pi} \left(\frac{\Omega_\chi \rho_c}{m_\chi} \right)^2 (1+z)^3 \frac{dN_\gamma}{dE_\gamma} e^{-\tau(E_\gamma, z)}. \quad (5)$$

By taking the ensemble average of Eq. (1), we obtain the isotropic background component of the intensity, $\langle I_\gamma(E_\gamma) \rangle$; it is equivalent to our evaluating $\langle \delta^2(z) \rangle$, the mean clumping factor of dark matter density fluctuations, which is given by the integral of two-point correlation over the momentum. We use a halo model approach (see Ref. [41] for a review) to calculate a reduced part of the N -point correlation function of density fluctuations.

The clumping factor, $\langle \delta^2 \rangle$, is then given by³

$$\langle \delta^2(z) \rangle = \int_{M_{\min}}^{\infty} dM \frac{dn}{dM}(M, z) \left(\frac{M}{\Omega_m \rho_c} \right)^2 \times \int dV u^2(r|M, z), \quad (6)$$

where $u(r|M, z) = \rho(r|M, z)/M$ is the density profile divided by the halo mass M , dn/dM the halo mass function for which we use the expression given in Ref. [43]. This clumping factor $\langle \delta^2(z) \rangle$ is also known as an intensity multiplier (it is the same quantity as, e.g., $\Delta^2(z)$ of Ref. [20] and $f(z)$ of Ref. [21]).

We should comment on the boundary of the mass integral in Eq. (6). As the mass function falls exponentially toward large masses, the integral converges at high mass end; however, it actually diverges at low mass end, although only very weakly. This raises some questions regarding robustness of theoretical predictions for the mean intensity of CGB from dark matter annihilation. What determines the minimum mass, M_{\min} ? In principle, one should integrate the mass function down to the free-streaming scale or the Jeans mass of dark matter particles, below which there is no fluctuation in dark matter. For both neutralinos and MeV dark matter, the minimum mass is roughly on the order of the mass of Earth [44, 45, 46, 47], while it can vary by orders of magnitude depending on the precise value of the dark matter mass. (One should recalculate M_{\min} as a function of the dark matter mass [26] or any other particle physics parameters that affect the strength of interactions.) When gamma rays emerge from annihilation without any other interactions of the products of annihilation with the materials within halos — i.e., dark matter annihilating directly into photons, photons emerge as the final state radiation of annihilation (also known as the internal bremsstrahlung), or decay of the products of annihilation into gamma rays (e.g., decay of π^0 produced by annihilation of neutralinos), one should use the minimum mass set by the free-streaming mass or the Jeans mass of dark matter particles. On the other hand, when gamma rays are produced predominantly by interactions between the products of annihilation and the materials within halos after annihilation, e.g., dark matter annihilation producing intermediate particles such as positrons which, in turn, annihilate with electrons *in the halo* to produce gamma rays, the minimum mass would be set by the Jeans mass of *baryons*, which is on the order of $10^6 M_\odot$ or larger [48]. Therefore, which minimum mass to use depends on what radiative processes one assumes for the production of gamma rays per annihilation.

³ The expression (6) is identical to the 1-halo term $I_{11}^{(1)}$ of Eq. (2.15a) in Ref. [42]. The second (2-halo) term $I_{12}^{(2)}$ disappears, because we evaluate the quantity at one point and halos are assumed to be exclusive, having stiff boundary.

This issue is further complicated by the fact that not all dark matter halos would actually survive during the formation of large-scale structure. Halos above the baryonic Jeans mass would survive without any problems; however, a significant fraction of halos with very small free-streaming masses, say $10^{-6}M_{\odot}$, would have been tidally disrupted shortly after their formation and might not be able to contribute to the CGB. The critical mass above which the tidal disruption due to hierarchical clustering becomes inefficient is difficult to calculate accurately at present [49, 50]. (Note that we are not concerned about the tidal disruption of these micro halos within larger halos — this would be a subject of the effect of substructures within halos, and we shall come back to this point in Sec. V C. Here, we are mostly concerned about the tidal disruption of the extragalactic micro halos that are outside of larger halos.)

Generally, the dependence of CGB anisotropy on the minimum mass is expected to be not very strong, when the amplitude of anisotropy is divided by the mean intensity, $\delta I_{\gamma}/\langle I_{\gamma} \rangle$, the dependence approximately canceling out in the numerator and denominator. To take into account the uncertainty in our understanding of the minimum mass contributing to the CGB, we explore two cases, $M_{\min} = 10^6 M_{\odot}$ and $10^{-6} M_{\odot}$, i.e., 12 orders of magnitude variation in the minimum mass.

The clumping factor depends on z through the halo mass function [43] and the concentration of density profiles [51, 52]. To compute the linear power spectrum that is necessary for the halo mass function, we adopt the fitting formula in Ref. [53]. The concentration parameter as a function of halo mass and redshift determines how steeply dark matter distributes in a halo; we use the result given in Ref. [51]. Using these ingredients, we compute the clumping factor for a given density profile. For the Navarro-Frenk-White (NFW) profile [54, 55] ($\gamma = 1$, where γ is defined by $\rho \propto r^{-\gamma}$ for small radii), we obtain $\langle \delta^2(0) \rangle \sim 4 \times 10^4$ for $M_{\min} = 10^6 M_{\odot}$ and 3×10^5 for $M_{\min} = 10^{-6} M_{\odot}$. For steeper profiles such as the one with $\gamma = 1.5$ suggested by the other simulations [56], the clumping factor increases by about an order of magnitude. More recent simulations suggest that γ depends on radii and could be anywhere between 1 and 1.5 in the inner region [57, 58, 59] (see also Refs. [60, 61, 62] for analytical approaches). Again, while the mean intensity depends strongly on γ (see, e.g., Ref. [26]), anisotropy (divided by the mean intensity) is expected to be less sensitive to the precise value of γ . For definiteness we adopt $\gamma = 1$ throughout the paper. Incidentally, it is practically useful to use the NFW profile, as many quantities used in the formalism can be calculated analytically for this profile.

One also needs to specify the particle physics parts involved in the function W — the dark matter mass, averaged cross section $\langle \sigma v \rangle$, and gamma-ray spectrum per annihilation. We assume that the dark matter particle contributing to the CGB totally accounts for the observed dark matter mass density, $\Omega_{\chi} = 0.23$. In many

cases, the annihilation cross section is closely related to Ω_{χ} , as it determines the abundance of dark matter particles having survived pair annihilation in the early universe.⁴ For both the supersymmetric neutralino and MeV dark matter, the canonical value of the cross section is $\langle \sigma v \rangle = 3 \times 10^{-26} \text{ cm}^3 \text{ s}^{-1}$, while a wide range of parameter space is still allowed⁵; in addition, we assume it to be independent of the relative velocity. Once again, the value of the annihilation cross section actually does not affect the CGB anisotropy, when it is normalized by the mean intensity, $\delta I_{\gamma}/\langle I_{\gamma} \rangle$. (The cancellation is exact when it is independent of velocity.) Thus, although a larger cross section is favored in order to make the dark matter contribution to the CGB mean intensity more significant, the prediction for the amplitude of anisotropy (divided by the mean intensity) is robust regardless of the precise value of the cross section.

While the energy spectrum of gamma-ray emission per annihilation contains rich information about the nature of dark matter particles, we do not pay much attention to the detailed shape of the spectrum, but rather simply split the spectrum into two parts: MeV and GeV regions, the former representing MeV dark matter, and the latter representing neutralinos. This is a reasonable approximation, as each contribution gives continuum gamma-ray emission that is roughly constant over relevant energy regions. For neutralinos we use a simple parameterization, $dN_{\gamma}/dE_{\gamma} \simeq (0.73/m_{\chi})e^{-7.76E_{\gamma}/m_{\chi}}/[(E_{\gamma}/m_{\chi})^{1.5} + 0.00014]$ [19]. The Kaluza-Klein dark matter particle might also contribute to the CGB in GeV region; their contribution may be calculated using an appropriate gamma-ray energy spectrum per annihilation. For MeV dark matter we consider the internal bremsstrahlung ($\chi\chi \rightarrow e^+e^-\gamma$) as the source of continuum emission, which gives $dN_{\gamma}/dE_{\gamma} = \alpha[\ln(s'/m_e^2) - 1][1 + (s'/s)^2]/(\pi E_{\gamma})$, where $\alpha = 1/137$ is the fine structure constant, $s = 4m_{\chi}^2$, and $s' = 4m_{\chi}(m_{\chi} - E_{\gamma})$ [34]. We shall ignore the 511 keV line emission, as its contribution must be subdominant compared with the AGN contribution [26].

In Fig. 1, we show the average CGB intensity calculated with the ingredients given above for the neutralino ($m_{\chi} = 100 \text{ GeV}$) and MeV dark matter ($m_{\chi} = 20 \text{ MeV}$). We also show the observational data obtained by the Imaging Compton Telescope (COMPTEL) [18] and

⁴ This would not be quite true when co-annihilations of dark matter particles with other particles dominate (e.g., neutralinos co-annihilating with other supersymmetric particles). In such a case the annihilation cross section would have little to do with Ω_{χ} . See Ref. [4] for more details.

⁵ For MeV dark matter, it has been argued that the canonical, velocity-independent cross section would overproduce the Galactic 511 keV emission [33, 63]. However, uncertainty in our understanding of the dark matter profile of our Galaxy still allows for the canonical cross section for $m_{\chi} \gtrsim 20 \text{ MeV}$ [26, 27]. If, on the other hand, m_{χ} turns out to be less than 20 MeV, then a smaller cross section may be preferred.

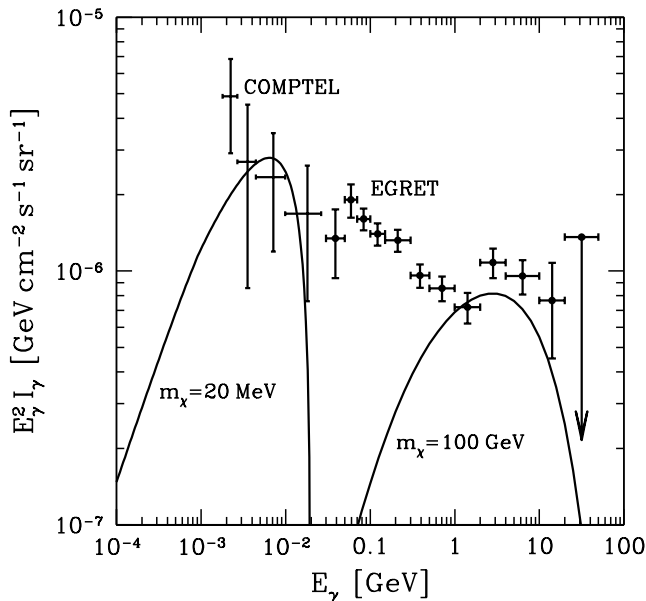


FIG. 1: Average intensity of the CGB from dark matter annihilation compared with the COMPTEL and EGRET data. The curve in GeV region is the predicted intensity for neutralinos with $m_\chi = 100$ GeV, while that in MeV region is the prediction for MeV dark matter particles with $m_\chi = 20$ MeV. As for the normalization, we have used $\langle\sigma v\rangle = 3 \times 10^{-26} \text{ cm}^3 \text{ s}^{-1}$, and extra “boost” factors have been multiplied to match the observational data. For details of the boost factors, see the last paragraph of Sec. II.

EGRET [15]. The predicted spectra have been multiplied by a factor of 1.5×10^3 (2.4×10^2) for the neutralino, and 10 (1.6) for the MeV dark matter, respectively, assuming $M_{\text{min}} = 10^6 M_\odot$ ($10^{-6} M_\odot$), to reasonably match the observational data. These boost factors may originate from dark matter substructures within halos or the cross section potentially larger than the value adopted here. Note that the 20 MeV dark matter with $M_{\text{min}} = 10^{-6} M_\odot$ (which is not very far away from the actual free-streaming mass of 20 MeV dark matter particles) can already account for most of the observed CGB without the need for a substantial boost due to substructures (the boost factor is only 1.6), which agrees with a more detailed analysis performed in Ref. [27].

III. COSMIC GAMMA-RAY BACKGROUND ANISOTROPY

In this section, we develop the formalism to analytically calculate the angular power spectrum of CGB anisotropy due to annihilation of dark matter particles. We note that this formalism is quite general, and with some modification, it can be applied to other situations including gamma rays from ordinary astrophysical ob-

jects.

A. General setup

We expand the deviation of CGB intensity from its mean value into the spherical harmonics coefficients, a_{lm} ,

$$\delta I_\gamma(\hat{\mathbf{n}}) \equiv I_\gamma(\hat{\mathbf{n}}) - \langle I_\gamma \rangle = \langle I_\gamma \rangle \sum_{lm} a_{lm} Y_{lm}(\hat{\mathbf{n}}). \quad (7)$$

Note that we have defined a_{lm} as a dimensionless quantity; thus, a_{lm} represents the amplitude of anisotropy divided by the mean intensity. Using the orthonormal relation of $Y_{lm}(\hat{\mathbf{n}})$, one obtains

$$\begin{aligned} \langle I_\gamma \rangle a_{lm} &= \int d\hat{\mathbf{n}} \delta I_\gamma(\hat{\mathbf{n}}) Y_{lm}^*(\hat{\mathbf{n}}) \\ &= \int d\hat{\mathbf{n}} \int dr f(r, \hat{\mathbf{n}} r) W(r) Y_{lm}^*(\hat{\mathbf{n}}), \end{aligned} \quad (8)$$

where

$$f \equiv \delta^2 - \langle \delta^2 \rangle, \quad (9)$$

and the energy index in the function W has been suppressed to simplify the notation.

The goal of the present paper is to evaluate the angular power spectrum, $C_l \equiv \langle |a_{lm}|^2 \rangle$, which is given by

$$\langle I_\gamma \rangle^2 C_l = \int \frac{dr}{r^2} \{W([1+z]E_\gamma, r)\}^2 P_f\left(k = \frac{l}{r}; r\right). \quad (10)$$

The detailed derivation of this result is given in Appendix A. Here, $P_f(k)$ is the three-dimensional (3D) power spectrum of f , defined by

$$\langle \tilde{f}_{\mathbf{k}} \tilde{f}_{\mathbf{k}'} \rangle = (2\pi)^3 \delta^{(3)}(\mathbf{k} + \mathbf{k}') P_f(k), \quad (11)$$

where $\delta^{(N)}$ represents the N -dimensional delta function, and $\tilde{f}_{\mathbf{k}}$ is the Fourier transform of $f(\mathbf{r})$. Note that \mathbf{k} is a comoving wavenumber, as it is a Fourier variable corresponding to the comoving distance \mathbf{r} . Given this relation (10), we first focus on deriving the 3D power spectrum, $P_f(k)$, and then turn to evaluating the angular power spectrum.

B. Three-dimensional power spectrum

1. Two-point contribution

The power spectrum, $P_f(k)$, is the Fourier transform of the two-point correlation function of f in real space, $\xi_f^{(2)}(\mathbf{x} - \mathbf{y}) \equiv \langle f(\mathbf{x}) f(\mathbf{y}) \rangle$. As f is a quadratic function of δ , $\xi_f^{(2)}$ is given by the two- and four-point correlation functions of δ , $\xi^{(2)}$ and $\xi^{(4)}$, as

$$\xi_f^{(2)}(\mathbf{x} - \mathbf{y}) = \xi^{(4)}(\mathbf{x}, \mathbf{x}, \mathbf{y}, \mathbf{y}) + 2\xi^{(2)}(\mathbf{x} - \mathbf{y})^2, \quad (12)$$

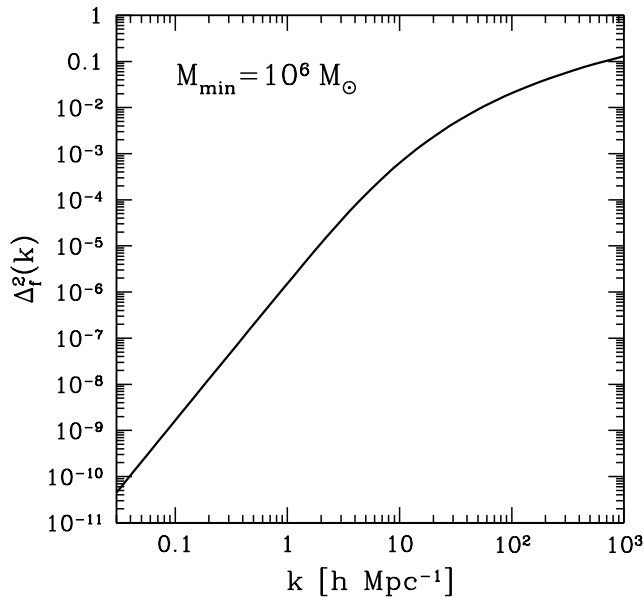


FIG. 2: Dimensionless power spectrum of $f = \delta^2 - \langle \delta^2 \rangle$, $\Delta_{f,2}^2(k)$ [Eq. (15)], from the two-point correlation term [Eq. (14)], evaluated at $z = 0$ for $M_{\min} = 10^6 M_{\odot}$.

where we have suppressed the label r (or equivalently z) to simply the notation. This motivates our decomposing the power spectrum into two parts as

$$P_f(k) = P_{f,4}(k) + P_{f,2}(k), \quad (13)$$

the first and second terms representing the contribution from the four- and two-point correlation parts, respectively. Since $\xi^{(2)}$ is related to the power spectrum of density fluctuations, $P(k)$, through the Fourier transformation, the second term, $P_{f,2}(k)$, is given by

$$P_{f,2}(k) = 2 \int \frac{d^3p}{(2\pi)^3} P(p)P(|\mathbf{k} - \mathbf{p}|). \quad (14)$$

Note that $P(k)$ is the *non-linear* power spectrum of density fluctuations. We calculate it using a halo model approach [64] (see also Appendix B). Figure 2 shows the two-point correlation contribution to the “dimensionless power spectrum” of f , evaluated at $z = 0$ for $M_{\min} = 10^6 M_{\odot}$; the quantity $\Delta_f^2(k)$ is defined by

$$\Delta_f^2(k) \equiv \frac{k^3}{2\pi^2} \frac{P_f(k)}{\langle \delta^2 \rangle^2}. \quad (15)$$

2. Four-point contribution

The four-point correlation function in Eq. (12) is further divided into 1-halo and 2-halo contributions,

$$\xi^{(4)}(\mathbf{x}, \mathbf{x}, \mathbf{y}, \mathbf{y}) = I_{1111}^{(1)} + I_{1122}^{(2)}. \quad (16)$$

The “1-halo term” represents correlations between particles within the same halo, whereas the “2-halo term” represents correlations between particles in two distinct halos. In other words, two points considered, \mathbf{x} and \mathbf{y} , are in one same halo for the 1-halo term, and are in two distinct halos for the 2-halo term.⁶ The corresponding power spectrum will be denoted as $P_{f,4}(k) = P_{f,4}^{1h}(k) + P_{f,4}^{2h}(k)$. According to Ref. [42], the 1-halo and 2-halo terms of the two-point correlation function are given respectively by

$$I_{1111}^{(1)} = \int_{M_{\min}}^{\infty} dM \frac{dn}{dM} \left(\frac{M}{\Omega_m \rho_c} \right)^4 \int d\mathbf{x}_1 \times u^2(\mathbf{x} - \mathbf{x}_1|M)u^2(\mathbf{y} - \mathbf{x}_1|M), \quad (17)$$

$$I_{1122}^{(2)} = \int_{M_{\min}}^{\infty} dM_1 \frac{dn}{dM_1} \int_{M_{\min}}^{\infty} dM_2 \frac{dn}{dM_2} \left(\frac{M_1 M_2}{\Omega_m^2 \rho_c^2} \right)^2 \times \int d\mathbf{x}_1 \int d\mathbf{x}_2 u^2(\mathbf{x} - \mathbf{x}_1|m_1) \times u^2(\mathbf{y} - \mathbf{x}_2|m_2)\xi_{hh}^{(2)}(\mathbf{x}_1, \mathbf{x}_2|M_1, M_2), \quad (18)$$

where $\xi_{hh}^{(2)}(\mathbf{x}_1, \mathbf{x}_2|M_1, M_2)$ is the two-point correlation function of halos of mass M_1 and M_2 , which is given by $\xi_{hh}^{(2)}(r|M_1, M_2) \approx b(M_1)b(M_2)\xi_{\text{lin}}^{(2)}(r)$ [$b(M)$ is the linear halo bias and $\xi_{\text{lin}}^{(2)}$ is the linear correlation function]. Equations (17) and (18) are then Fourier transformed, giving the power spectrum as follows:

$$P_{f,4}^{1h}(k) = \int_{M_{\min}}^{\infty} dM \frac{dn}{dM} \left(\frac{M}{\Omega_m \rho_c} \right)^2 v^2(k|M), \quad (19)$$

$$P_{f,4}^{2h}(k) = \left[\int_{M_{\min}}^{\infty} dM \frac{dn}{dM} \left(\frac{M}{\Omega_m \rho_c} \right) b(M)v(k|M) \right]^2 \times P^{\text{lin}}(k), \quad (20)$$

where $v(k|M)$ is the Fourier transform of $u^2(\mathbf{x}|M)M/\Omega_m \rho_c$, which is analytically solvable for the NFW profile with fairly a lengthy expression, and shown in Fig. 3 for various values of M . Note that these expressions are identical to those for the ordinary matter power spectrum, Eqs. (B1) and (B2), if we replace $v(k|M)$ by $u(k|M)$.

Figure 4 shows the dimensionless power spectrum from the four-point contribution, $\Delta_{f,4}^2(k)$, evaluated at $z = 0$ for $M_{\min} = 10^6 M_{\odot}$. We find that the four-point term always dominates over the two-point term at all wavenumbers; thus, the two-point contribution may be safely ignored. The 1-halo term dominates at smaller spatial scales, $k \gtrsim 2 h \text{ Mpc}^{-1}$, whereas the 2-halo term dominates at larger scales.

⁶ The full expression of $\xi^{(4)}$ contains one 1-halo, six 2-halo, seven 3-halo, and one 4-halo terms [42]. However, most of them are vanishingly small for a particular configuration considered here, $\xi^4(\mathbf{x}, \mathbf{x}, \mathbf{y}, \mathbf{y})$, as halos are spatially exclusive — the same reason as that stated in the second footnote.

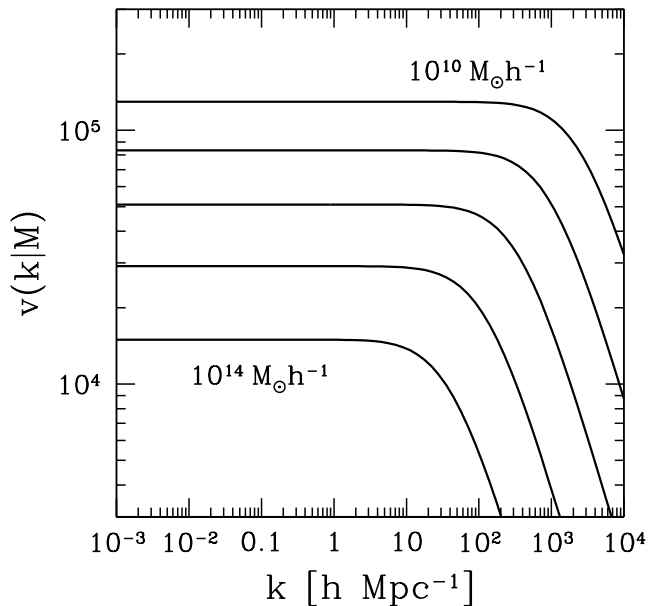


FIG. 3: The function that determines the four-point contribution to the power spectrum of CGB anisotropy, $v(k|M)$ [see Eqs. (19) and (20)], as a function of k evaluated at $z = 0$ for various values of M . The value of M labeling each curve is spaced by one order of magnitude, with the largest and smallest values as indicated.

In Fig. 5, we plot $\Delta_f^2(k)$ at $z = 0$ for the smaller minimum mass, $M_{\min} = 10^{-6} M_{\odot}$. The contributions from halos whose masses are in some specific ranges are also shown. We find an interesting trade-off between large and small mass halos. Larger mass halos give much larger 1-halo term contributions and thus completely dominate $\Delta_f^2(k)$ at small scales. On the other hand, smaller mass halos give much larger 2-halo term contributions and thus completely dominate $\Delta_f^2(k)$ at large scales. This phenomena results in a “break” in the shape of $\Delta_f^2(k)$ at a critical wavenumber, $k \sim 1\text{--}10 h \text{ Mpc}^{-1}$ depending on M_{\min} , below which the dominant contribution to $\Delta_f^2(k)$ comes from the smallest halos, and above which the dominant contribution comes from the largest halos.

We find by comparing Figs. 4 and 5 that the 2-halo contribution to $\Delta_f^2(k)$ is virtually unaffected by M_{\min} . This is somewhat surprising, given that the 2-halo contribution is dominated by the smallest halos having M_{\min} . The reason for this phenomenon is because we define $\Delta_f^2(k)$ as a ratio of $P_f(k)$ and the clumping factor squared, $\langle \delta^2 \rangle^2$ [see Eq. (15)]. Reducing the minimum mass increases *both* $P_f(k)$ and $\langle \delta^2 \rangle^2$ by the same amount, which makes the 2-halo contribution nearly independent of the choice of M_{\min} . On the other hand, the 1-halo contribution decreases as M_{\min} decreases. This is easy to understand. As the 1-halo contribution to $P_f(k)$ is entirely dominated by the largest halos, it is

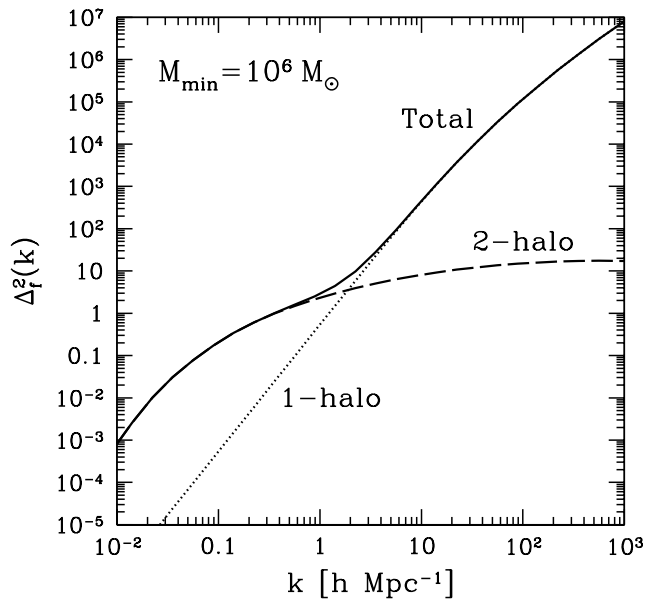


FIG. 4: Dimensionless power spectrum of $f = \delta^2 - \langle \delta^2 \rangle$ from the four-point contribution, $\Delta_{f,4}^2(k)$ [Eq. (15)], by the 1-halo (dotted) and 2-halo (dashed) terms [Eqs. (19) and (20)]. Both are evaluated at $z = 0$ for $M_{\min} = 10^6 M_{\odot}$.

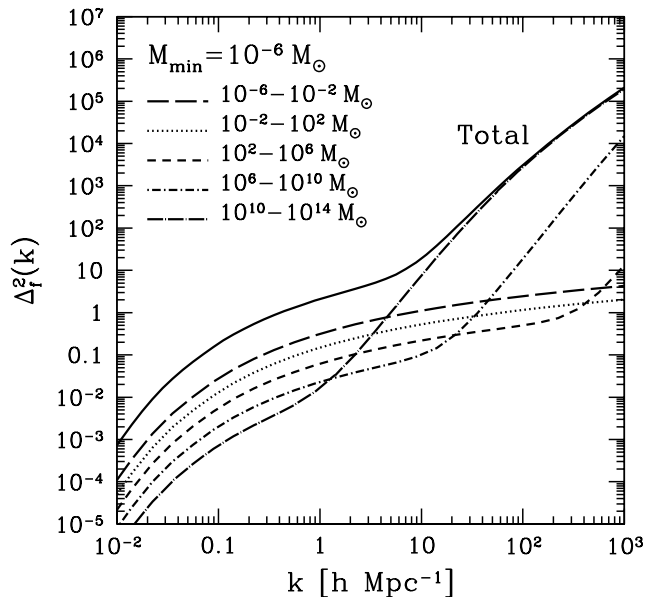


FIG. 5: The same as Fig. 4 but for the smaller minimum mass, $M_{\min} = 10^{-6} M_{\odot}$. Contributions from halos of various mass ranges are also shown.

independent of M_{\min} ; however, as the clumping factor increases for smaller M_{\min} , the dimensionless power spectrum, $\Delta_f^2(k) \propto P_f(k)/\langle\delta^2\rangle^2$, decreases for smaller M_{\min} . As a result, a smaller M_{\min} makes the shape of $\Delta_f^2(k)$ flatter, reducing the power at larger k . A “shoulder” due to the 2-halo term then becomes more prominent for smaller M_{\min} , which is a characteristic that may be observable in the angular anisotropy, as we discuss in the next section.

IV. ANGULAR POWER SPECTRUM

By using Eq. (10) with the 3D power spectrum shown in Figs. 4 and 5, we can calculate the angular power spectrum, C_l , as a function of multipoles, l , for a given dark matter model. We here note that C_l roughly corresponds to the correlation between two points on the sky separated by an angle $\theta \approx \pi/l$.

A. Supersymmetric neutralino

First, we consider supersymmetric neutralinos as the dark matter candidate, and assume that the neutralino mass is 100 GeV. While the mean intensity, $\langle I_\gamma \rangle$, is very sensitive to the dark matter mass, $\langle I_\gamma \rangle \propto m_\chi^{-2}$, this factor exactly cancels out when the amplitude of anisotropy is divided by the mean intensity. Thus, C_l depends on m_χ only weakly through the mass dependence of the gamma-ray spectrum per annihilation. We evaluate the anisotropy power per logarithmic range of l , $l(l+1)C_l/2\pi$.

In Figs. 6(a) and 6(b), we show the predicted angular power spectrum evaluated at the observed gamma-ray energy of $E_\gamma = 10$ GeV for $M_{\min} = 10^6 M_\odot$ and $10^{-6} M_\odot$, respectively. One can understand the shape of the angular spectrum for both cases using the same argument for understanding the shape of the 3D dimensionless power spectrum, $\Delta_f^2(k)$, in the previous section. A rapid increase in C_l at small angular scales (large l) is due to the 1-halo term contribution. The 1-halo term dominates even at relatively small l , $l \sim 10$, for the larger minimum mass, whereas it is suppressed significantly for the smaller minimum mass, in agreement with the dependence of the shape of $\Delta_f^2(k)$ on M_{\min} that we discussed in the previous section. On the other hand, the 2-halo term contribution is nearly independent of M_{\min} , which is also in agreement with $\Delta_f^2(k)$. (The 1-halo term is roughly proportional to the inverse of the clumping factor squared, while the 2-halo term is nearly independent of the clumping factor.) This peculiar dependence of the shape of C_l on M_{\min} opens up an exciting possibility that one can “measure” the minimum mass from the shape of C_l . Together with the information from the energy spectrum of the CGB, therefore, it may be possible to identify the mechanism by which gamma rays are produced from annihilation of dark matter and the degree to which small halos are tidally disrupted by the structure formation.

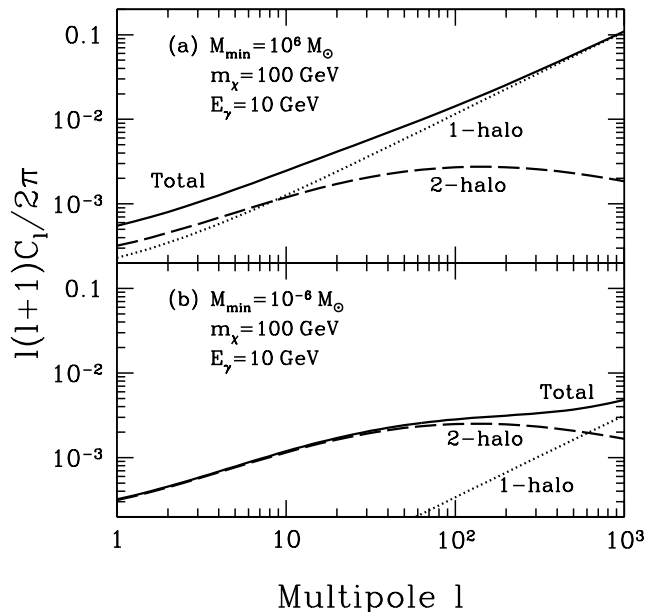


FIG. 6: Angular power spectrum of the CGB, C_l , from annihilation of supersymmetric neutralinos, evaluated for (a) $M_{\min} = 10^6 M_\odot$ and (b) $M_{\min} = 10^{-6} M_\odot$. Note that C_l is dimensionless: the mean intensity squared should be multiplied in order to convert it to the units of intensity squared. The neutralino mass m_χ is assumed to be 100 GeV. The predicted angular spectrum is shown at the observed gamma-ray energy of $E_\gamma = 10$ GeV. Contributions to C_l from the 1-halo (dotted) and 2-halo (dashed) terms are shown as well as the total signal (solid).

Is the predicted angular power spectrum detectable? We compare the predicted power spectrum with the expected sensitivity of the GLAST experiment. We take the following specifications for GLAST: the field of view is $\Omega_{\text{fov}} = 4\pi f_{\text{fov}} = 2.4$ sr, the angular resolution is $\sigma_b = 0.115^\circ$, and the effective area is $A_{\text{eff}} = 10^4$ cm² at 10 GeV [65]. Note that the angular resolution is defined as a half width of a Gaussian point spread function, and the full width at half maximum is given by $\sqrt{8 \ln 2} \sigma_b$. In addition, for the diffuse gamma-ray observation, the background contamination can be reduced to 6% of the CGB, which is a promising characteristic [65]. Therefore, a fractional error of C_l ,

$$\frac{\delta C_l}{C_l} = \sqrt{\frac{2(1 + C_{N,\gamma}/W_l^2 C_l)^2}{(2l+1)\Delta l f_{\text{fov}}}}, \quad (21)$$

is essentially determined by the Poisson noise of the cosmic signal. Here Δl is the bin width of l (we choose $\Delta l = 0.3l$ for $M_{\min} = 10^6 M_\odot$ and $0.5l$ for $10^{-6} M_\odot$), $C_{N,\gamma} = \Omega_{\text{fov}}[(N_N/N_\gamma)^2/N_N + 1/N_\gamma]$ is the power spectrum of photon noise, N_N and N_γ are the count number of backgrounds and the signal ($N_N/N_\gamma \ll 1$ for GLAST), respectively, and W_l is the window function of a Gaus-

sian point spread function, $W_l = \exp(-l^2\sigma_b^2/2)$. If we assume that the CGB detected in GeV region is dominated by gamma rays from dark matter annihilation, we may use the observed CGB intensity, $E_\gamma^2\langle I_\gamma \rangle = 1.5 \times 10^{-6}$ GeV cm $^{-2}$ s $^{-1}$ sr $^{-1}$ [14, 15], to estimate the signal-to-noise for anisotropy. The expected number of photons, N_γ , for GLAST would then be $N_\gamma = E_\gamma\langle I_\gamma \rangle\Omega_{\text{fov}}A_{\text{eff}}t = 10^3(t/1 \text{ yr})$ at $E_\gamma = 10$ GeV, while N_N is negligible.

In Fig. 7, we show the predicted angular power spectrum at the observed gamma-ray energies of $E_\gamma = 3, 10,$ and 20 GeV, assuming $M_{\text{min}} = 10^6 M_\odot$, with the expected 1σ errors of C_l at $E_\gamma = 10$ GeV for $t = 1$ yr of observations. We find that the GLAST should be able to measure the angular power spectrum of the CGB fairly easily for 1 year of observations, if the dark matter particle is the neutralino with mass around 100 GeV and its annihilation dominates the observed CGB in GeV region. The angular power spectrum for the smaller minimum mass, $M_{\text{min}} = 10^{-6} M_\odot$ is shown in Fig. 8, with the expected error bars. We find that anisotropy is still easily detectable with the GLAST for 1 year of observations. Therefore, we conclude that, if dark matter particles are supersymmetric neutralinos and the observed CGB in GeV region is dominated by their annihilation, the GLAST should be able to measure the angular power spectrum of CGB anisotropy, regardless of the minimum mass.

As prospects for detecting CGB anisotropy in the GLAST data are very good, it is tempting to speculate that one may actually detect CGB anisotropy in the existing EGRET data. The EGRET parameters are $\Omega_{\text{fov}} = 0.5$ sr, $\sigma_b = 0.5^\circ$, and $A_{\text{eff}} = 7 \times 10^2$ cm 2 at 10 GeV and on-axis direction (A_{eff} decreases by a factor of 2 at 20° and of 6 at 30°) [66]. The background noise has been suppressed by an order of magnitude compared with the photon counts from the CGB. Although the detector sensitivity of the EGRET is not as good as that of the GLAST, we expect that the Poisson error (photon noise) of the signal to be quite small at $l \lesssim 400$ owing to a longer integration time (EGRET has observed the sky for much more than 1 year). The data above $l \approx 400$ would not be very useful because of the limited angular resolution. While one needs to carefully characterize the systematic uncertainty due to the Galactic foreground removal, the power spectrum of CGB anisotropy in the EGRET data should be measured in search of the signatures of dark matter annihilation.

B. MeV dark matter

As for the MeV dark matter, the continuum gamma rays are emitted by the internal bremsstrahlung, and the spectrum shape is shown in Sec. II (see also, Refs. [27, 34]). Figure 9 shows the predicted angular power spectrum of CGB anisotropy for the MeV dark matter with $m_\chi = 20$ MeV. We show C_l at the observed gamma-ray energy of $E_\gamma = 3$ and 10 MeV, as well as the ex-

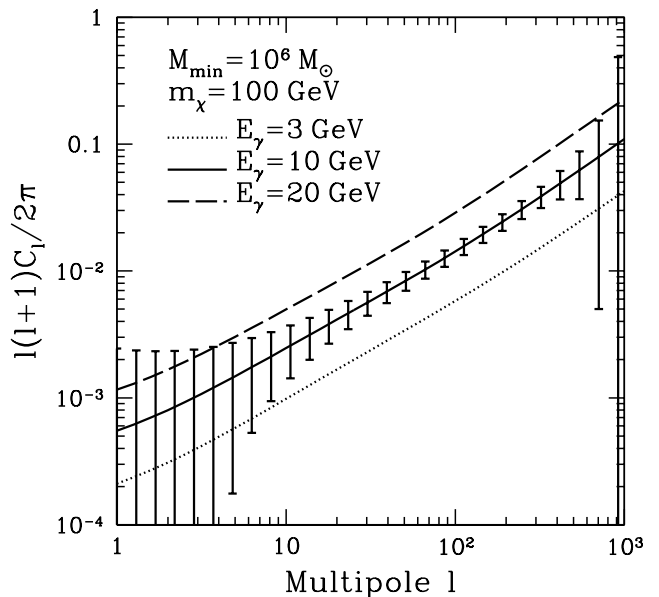


FIG. 7: Angular power spectrum of the CGB, C_l , from annihilation of supersymmetric neutralinos, evaluated for $M_{\text{min}} = 10^6 M_\odot$. The neutralino mass m_χ is assumed to be 100 GeV. The predicted angular spectrum is shown at the observed gamma-ray energy of $E_\gamma = 3, 10,$ and 20 GeV. The 1σ error bars of C_l expected from GLAST for 1 year of operation are also shown at $E_\gamma = 10$ GeV.

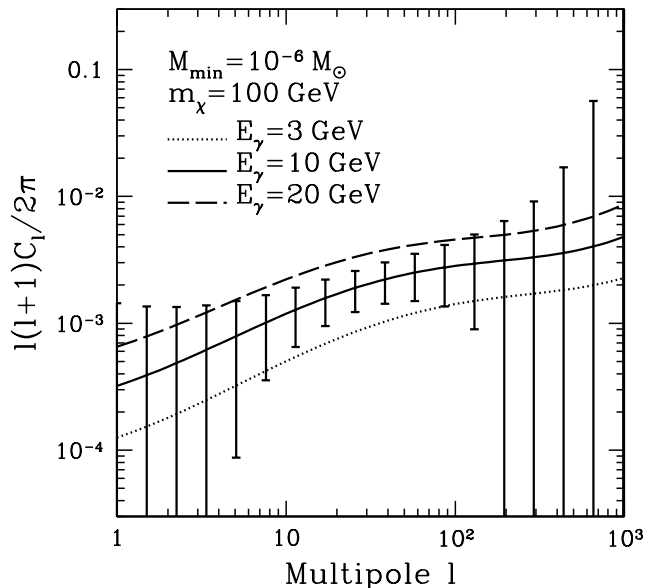


FIG. 8: The same as Fig. 7, but evaluated for the smaller minimum mass, $M_{\text{min}} = 10^{-6} M_\odot$, which is closer to the free-streaming mass of neutralinos. (Note that the precise value of the free-streaming mass depends strongly on the dark matter mass and interaction properties.)

pected uncertainty at 10 MeV. The shape as well as the normalization are very similar to those for the neutralinos. In the MeV regime, the most promising technique to detect gamma rays is the Compton scattering inside the detector. Although the design of future detectors of this kind, such as the Advanced Compton Telescope (ACT) [67], are still in progress, we parameterize it with $\sigma_b = 1^\circ$, $A_{\text{eff}} = 100 \text{ cm}^2$, $\Omega_{\text{fov}} = 1 \text{ sr}$, $t = 1 \text{ yr}$, and $N_N/N_\gamma = 1$ [38]. Again taking the mean CGB intensity at 10 MeV to be what has been observed, $10^{-4} \text{ cm}^{-2} \text{ s}^{-1} \text{ sr}^{-1}$ [16, 17, 18], the signal count with ACT would be $N_\gamma = 3 \times 10^5 (t/1 \text{ yr})$. With these parameters for ACT, we find that it should be easy to measure the power spectrum in the range of $10 < l < 100$. Above $l = 100$, the errors become exponentially larger because of the detector angular resolution, i.e., due to the effect of the window function W_l in Eq. (21); this is unavoidable unless better angular resolution is realized.

The dependence of C_l on the minimum mass, M_{min} , is almost the same as that for the neutralino. In Fig. 10, we show the angular power spectrum for the smaller minimum mass, $M_{\text{min}} = 10^{-6} M_\odot$. (And this is a correct mass to use, up to the dependence on the dark matter mass [26], when the emission is due to the internal bremsstrahlung; for the minimum mass appropriate for the 511 keV emission, see arguments in Ref. [48].) Again, the predicted angular power spectrum is well above the expected uncertainty, and thus our conclusion about prospects for detection of anisotropy is robust regardless of the minimum mass.

The COMPTEL has measured the CGB in this energy region [18]. The parameters of the COMPTEL are $\Omega_{\text{fov}} = 1 \text{ sr}$, $\sigma_b = 1.5^\circ$, $A_{\text{eff}} = 30 \text{ cm}^2$ at 20 MeV [68], which are almost comparable to the parameters adopted for the ACT. The biggest issue is, however, its poor signal-to-background ratio, $N_\gamma/N_N \approx 0.01$; thus, it would be quite challenging to detect CGB anisotropy in the COMPTEL data because of large statistical errors.

V. DISCUSSION

A. Dependence on gamma-ray energy

In addition to the shape of the angular power spectrum as a function of l , it would be useful to discuss dependence on the gamma-ray energy in order to obtain further information on the CGB origin. We show the energy spectrum of isotropic, $\langle I_\gamma \rangle$, and anisotropic, $\langle I_\gamma \rangle [l(l+1)C_l/(2\pi)]^{1/2}$, components of the CGB in units of intensity in Fig. 11(a), for both the neutralino ($m_\chi = 100 \text{ GeV}$) and MeV dark matter ($m_\chi = 20 \text{ MeV}$) assuming $M_{\text{min}} = 10^6 M_\odot$. The energy spectrum of anisotropy divided by the mean intensity, $l(l+1)C_l/(2\pi)$, is also shown in Fig. 11(b). We show only $l = 100$. The isotropic spectrum is boosted accordingly in order to explain the observed intensity; the details are given in the last paragraph of Sec. II.

We find that anisotropy is enhanced when the spec-

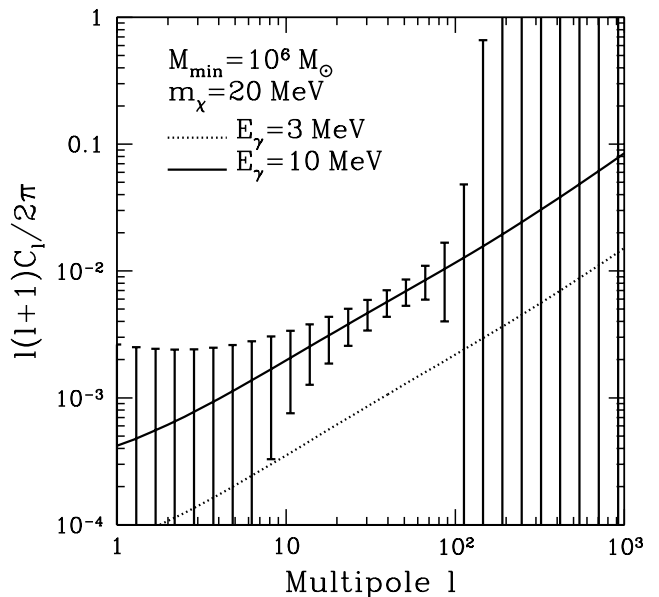


FIG. 9: The same as Fig. 7 but for MeV dark matter with $m_\chi = 20 \text{ MeV}$, evaluated at $E_\gamma = 3$ (dotted) and 10 (solid) MeV. Error bars are calculated for ACT in 1 year of operation.

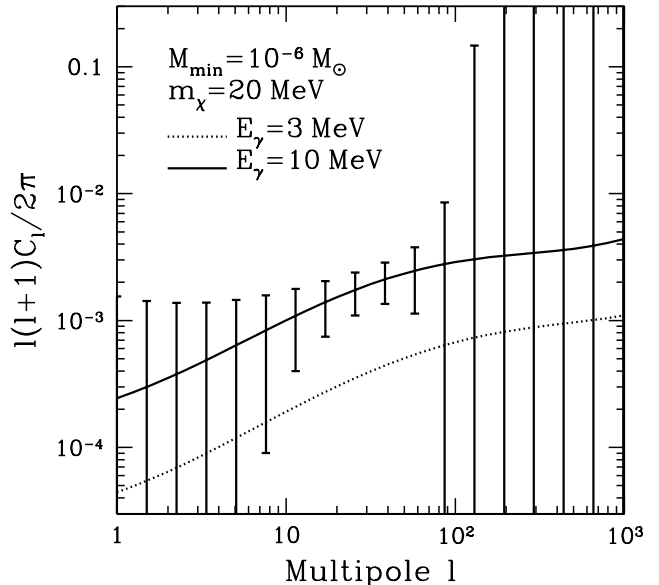


FIG. 10: The same as Fig. 9, but evaluated for the smaller minimum mass, $M_{\text{min}} = 10^{-6} M_\odot$, which is closer to the free-streaming mass of MeV dark matter. (Note that the precise value of the free-streaming mass depends strongly on the dark matter mass and interaction properties.)

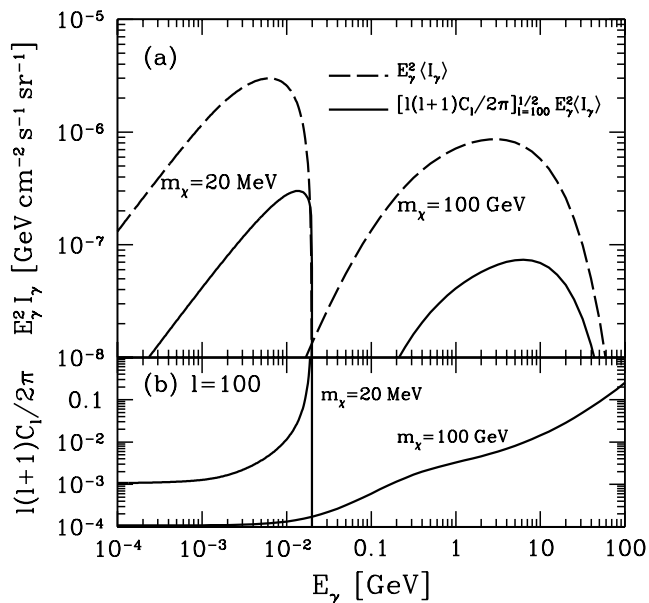


FIG. 11: (a) Energy spectrum of isotropic (dashed) and anisotropic (solid) component of the CGB intensity for $m_\chi = 100$ GeV (right curves) and 20 MeV (left curves), evaluated for $M_{\min} = 10^6 M_\odot$. Anisotropic components are evaluated at $l = 100$. (b) Energy spectrum of anisotropy divided by the mean intensity at $l = 100$.

trum has sharp features such as edges (as seen at ~ 20 MeV for the MeV dark matter case) or lines. This has been pointed out by Ref. [38] in the context of CGB anisotropy from Type Ia supernovae. Therefore, if the energy resolution of gamma-ray detectors is sufficiently good to resolve these properties, the spectral features would provide another powerful diagnosis of dark matter annihilation signals. The features might also allow us to obtain information on the redshift evolution of the sources (see, Ref. [38] for more details). Other potential spectrum signatures include the line gamma emission ($\chi\chi \rightarrow \gamma\gamma, Z^0\gamma$) and internal bremsstrahlung ($\chi\chi \rightarrow W^-W^+\gamma$ [69]) from annihilation of neutralinos, as well as the 511 keV line emission from annihilation of MeV dark matter particles into e^-e^+ pairs.

B. Other astrophysical sources

The angular power spectrum shown in Figs. 7–10 should be very characteristic of annihilating dark matter in extragalactic dark matter halos, as the gamma-ray intensity is proportional to the density squared. The intensity of gamma rays coming directly from other astrophysical sources should be linearly proportional to density. It is likely that blazars are the most dominant constituent of the GeV gamma rays over a wide energy range [70, 71]. Assuming that blazars are biased tracers of the underlying

ing mass distribution, the two-point correlation function of blazars should be simply given by that of density fluctuations, $P(k)$. For more quantitative study, we perform the following simple analyses for the power spectrum of blazars.

First, we assume that blazars are very rare objects and their angular spectrum is entirely dominated by the shot noise. In this case the angular power spectrum does not depend on l , and thus $l(l+1)C_l$ is proportional to l^2 at $l \gg 1$. We show in Figs. 12(a) and 12(b) that the shot noise spectrum totally lacks the power on large angular scales (i.e., the spectrum is too steep), and can be easily distinguished from dark matter annihilation.

Second, we take the other extreme limit where blazars are quite common and trace the underlying matter density field, δ , fairly well. Specifically, we calculate the line-of-sight integral in Eq. (1) with δ^2 replaced by δ . The volume emissivity is then given by $P_\gamma \propto \delta(1+z)^3 E_\gamma dN_\gamma/dE_\gamma$, and we assume a power-law blazar energy spectrum falling off as $dN_\gamma/dE_\gamma \propto E_\gamma^{-2}$ (e.g., [72] for Mrk 421), which gives $W(E_\gamma, z) \propto E_\gamma^{-2} e^{-\tau(E_\gamma, z)}$. We calculate the angular power spectrum, C_l , using Eq. (10) with $P_f(k)$ replaced by $P(k)$. Finally, we assume that blazars form only when the mass of host dark matter halos is larger than $M_{\min} = 10^{11} M_\odot$. In this simplified prescription, the average number of blazars in a halo linearly increases with the host halo mass. In reality, however, this may not be true and we may also need to take into account the difference between a central galaxy and satellite galaxies within a dark matter halo. This kind of galaxy distribution model, called the Halo Occupation Distribution (see Ref. [41] for a review), could be made more realistic for blazars; however, we do not pursue it in any more detail, and adopt the above model for calculating the angular power spectrum of gamma-ray emission from “blazars.”⁷

We show the shape of the angular power spectrum expected from blazars in Figs. 12(a) and 12(b). (Normalizations are taken arbitrarily.) The blazar power spectrum is determined by the 1-halo term at all multipoles; thus, the spectrum is nearly a power law with a little bit of flattening above $l \sim 200$, which is due to the minimum mass of halos hosting blazars, $10^{11} M_\odot$. The small-scale power drops as we raise the minimum mass of host halos (see, e.g., Fig. 2 of Ref. [64]). In Fig. 12(a), we compare the blazar spectrum with the spectrum of CGB anisotropy from annihilation of neutralinos with $m_\chi = 100$ GeV for the large minimum mass, $10^6 M_\odot$. As we have noted before, the annihilation spectrum for $M_{\min} = 10^6 M_\odot$ is also

⁷ Our model is probably not a very good model for describing the power spectrum of real blazars. It simply describes the angular power spectrum of dark matter halos above $10^{11} M_\odot$ which emit gamma rays (by whatever mechanism) with an energy spectrum falling off as $dN_\gamma/dE_\gamma \propto E_\gamma^{-2}$. In reality, not all dark matter halos above $10^{11} M_\odot$ host blazars, and blazars are known to be transient objects which turn on and off.

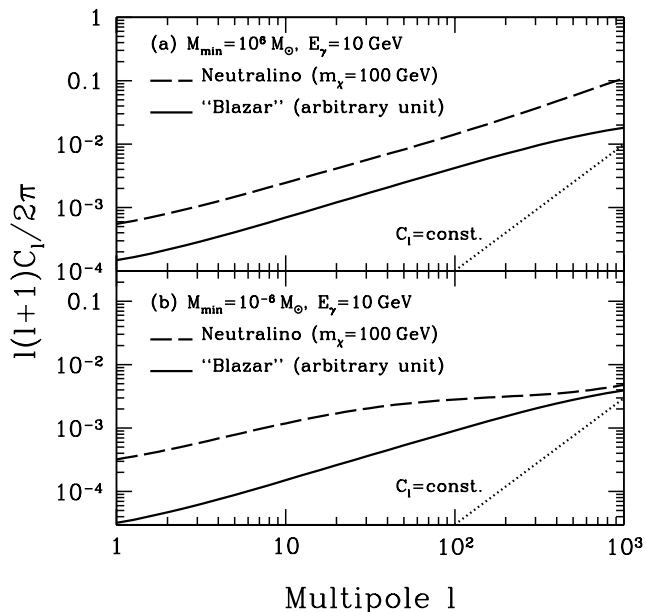


FIG. 12: Shape of the angular power spectrum of the CGB expected from unresolved “blazars” (solid lines; see the footnote 5 for the reason why the quotation marks are put) with arbitrary normalizations. The power spectrum from annihilation of neutralinos with $m_\chi = 100$ GeV is also plotted as the dashed lines. The adopted gamma-ray energy is 10 GeV, and the minimum mass of dark matter halo is (a) $10^6 M_\odot$, and (b) $10^{-6} M_\odot$. The dotted lines show the shot noise ($C_l = \text{const.}$) with arbitrary normalizations, which represent the power spectrum of very rare sources.

dominated by the 1-halo term at all multipoles, which makes the annihilation and blazar spectrum actually look similar at $l \lesssim 200$. Above $l \sim 200$, however, the annihilation spectrum continues to grow whereas the blazar spectrum flattens out. In Fig. 12(b), we use the smaller minimum mass, $10^{-6} M_\odot$, which is probably more realistic for dark matter annihilation. In this case the dominant contribution comes from the 2-halo term, which makes the annihilation spectrum substantially flatter than the blazar spectrum. In other words, the annihilation spectrum has much more power at large angular scales, which should be easily distinguished from the blazar spectrum. The same argument should also apply to the CGB in the MeV region from Type Ia supernovae. (See Ref. [38] for another approach to calculating the angular correlation function of Type Ia supernovae.)

Another potential astrophysical contributor to the CGB is the gamma-ray emission from particles accelerated by shock waves forming in galaxy clusters [73, 74, 75, 76, 77, 78]. There have been a few claims about detection of a correlation between the position of clusters and the EGRET data [79, 80]. When the gamma rays are emitted mainly by the inverse Compton scattering off the CMB photons by accelerated electrons,

which many authors considered to be the dominant emission process, the gamma-ray intensity would be proportional to the baryon density at the shock. On the other hand, when the gamma rays are produced by collisions between cosmic-ray protons (accelerated by the cluster shocks) and intracluster medium, the gamma-ray intensity would be proportional to the baryon density squared at the shock. However, the baryon density distribution at the shock would be very different from the distribution of dark matter particles. One would need cosmological hydrodynamical simulations to study the shape of the angular power spectrum of CGB from such processes.

C. Substructure of dark matter halos

The biggest uncertainty in calculations of the CGB, whether the mean intensity or anisotropy, is the substructure (i.e., small-scale clumpiness) within dark matter halos. N -body simulations of collisionless dark matter universally indicate the existence of sub-halo clumping of dark matter [81]. This effect has been entirely ignored in our calculations, as we have assumed that each halo has a smooth density profile. It is expected that the dark matter substructure increases the gamma-ray intensity by simply increasing the clumpiness.⁸ How much it is increased depends very much on the exact amount of substructure, which is difficult to predict due to a limited resolution of the current N -body simulations. In this regard, our calculations provide the lower limit to the angular power spectrum of CGB. The fact that our predictions are already well above the noise level of GLAST and ACT is extremely encouraging for prospects of detection of anisotropy.

Let us comment on some effects of dark matter substructures on the angular power spectrum. It is expected that the effect of substructure would be smaller for anisotropy than for the mean intensity, when the amplitude of anisotropy is divided by the mean intensity (which is what we have been using to calculate C_l). But still, the increased clumping will increase the four-point function of density fluctuations, particularly 1-halo term which dominates at small scales. Therefore, we expect the substructure to modify C_l at large l , while we do not expect a significant change in C_l at small l , where the four-point function is dominated by the 2-halo term. Finally, in the limit that dark matter annihilation signals are completely dominated by the sub-halos within a bigger (host) halo, e.g., Earth-mass micro halos in a Milky-Way size halo, the gamma-ray intensity may be *linearly* proportional to the density profile of host halos [25]. In this model, there is no gamma-ray emission from the intra-halo medium between the sub-halos, and the

⁸ For gamma rays from annihilation of dark matter in the substructure of our Galaxy, see Refs. [82, 83, 84, 85, 86, 87, 88].

sub-halos are assumed to follow the density profile of a host halo. Our formalism should be modified for this case by including the number of sub-halos within a host halo as a function of the host halo mass, which is essentially the Halo Occupation Distribution for the sub-halos.

Incorporating dark matter substructures into the halo model is an active field of research, and therefore we expect to be able to get a better handle on this effect in near future.

VI. CONCLUSIONS

The CGB provides indirect means to probe the nature of dark matter particles via high-energy photons from dark matter annihilation. The dark matter annihilation has occurred in all the past halos, and now contributes to the CGB flux at some level; its contribution might be dominant if the flux is boosted by some mechanism such as tidally survived dark matter substructure. Therefore, revealing the origin of the CGB is an very important problem that is potentially connected to the dark matter properties and halo substructure as well as ordinary astrophysical objects. In order to achieve this purpose, while the energy spectrum of the mean intensity of CGB has been investigated by many researchers, anisotropy of CGB from dark matter annihilation has been entirely neglected. In this paper we have calculated the angular power spectrum of CGB from dark matter annihilation for the first time, using an analytical halo model approach. As for dark matter candidates, we have discussed two possibilities: one is the supersymmetric neutralino, one of the most popular candidates today, which contributes to the CGB in GeV region. The other is the MeV dark matter, a dark matter species first introduced to explain the 511 keV emission line from the Galactic center by annihilation into e^-e^+ pair, which contributes to the CGB in MeV region.

Since the gamma-ray intensity from annihilation is proportional to the density squared, ρ_χ^2 , we have derived the 3D power spectrum of the quantity $f = \delta^2 - \langle \delta^2 \rangle$, $P_f(k)$. The calculation involves the Fourier transformation of the four-point correlation function of underlying mass density fluctuations, $\xi^{(4)}$, which has been shown to dominate over the two-point correlation contribution, $\xi^{(2)2}$. This $P_{f,4}(k)$ includes the 1-halo and 2-halo terms, the former containing two points within the same halo, and the latter containing two points in two different halos. The analytical expressions for $P_f(k)$ from each term are given in Eqs. (14), (19), and (20), and the results are plotted in Figs. 2, 4, and 5. At all scales the four-point contribution totally dominates the signal; at small scales, the 1-halo term dominates.

We note that our formalism can also be used for any other emission processes that involve collisions of two particles. For example, one may use this to compute the power spectrum of free-free or bound-free emission from the ionized gas in halos. For this application one

needs to replace the dark matter density profile with the gas density profile.

Using Eq. (10) that connects the 3D power spectrum, $P_f(k)$, to the angular power spectrum, C_l , we have calculated the CGB angular power spectrum as a function of multipoles, l , for both the neutralino ($m_\chi = 100$ GeV) and MeV dark matter ($m_\chi = 20$ MeV) at various gamma-ray energies. We have also compared the predicted signals with the expected sensitivity of future gamma-ray detectors — GLAST in GeV region (for neutralinos) and ACT in MeV region (for MeV dark matter). The results are shown in Figs. 7–10. For both cases, we have found that these detectors will have sufficient sensitivity to measure the angular power spectrum with reasonable accuracy.

We have studied the effects of the minimum mass, M_{\min} , on the predicted angular power spectrum in detail. While the 1-halo contribution, which dominates at small angular scales (large l), decreases for smaller M_{\min} , the 2-halo contribution, which dominates at large angular scales (small l), is virtually unaffected by M_{\min} . This property results in a peculiar dependence of the shape of C_l on M_{\min} , which may be used in combination with the information from the energy spectrum of the CGB to determine M_{\min} . As M_{\min} depends on the radiation processes of gamma rays from annihilation as well as the survival of micro halos contributing to the CGB, the shape of C_l provides a powerful tool for determining these properties, which are otherwise difficult to probe. Our conclusion about prospects for measuring C_l of CGB anisotropy are robust regardless of M_{\min} .

By applying our formalism with some modification, we have shown that the other astrophysical sources such as blazars would reveal a different shape of the angular power spectrum, as these contributions are linearly proportional to density fluctuations. The shape of C_l at large l might further change when we take into account the dark matter substructure, but the result in this paper sets a lower bound on anisotropy at all multipoles, which provides excellent prospects for detection of CGB anisotropy by future gamma-ray detectors.

We conclude that the angular power spectrum of CGB provides a smoking-gun signature for gamma-ray emission from annihilation of dark matter particles, which would be a powerful tool for understanding the nature of dark matter particles.

Acknowledgments

We would like to thank Kyungjin Ahn, John Beacom, Gianfranco Bertone, Celine Bøhm, Peter Michelson, and Tomonori Totani for valuable comments. We would also like to thank Duane E. Gruber for providing us with the COMPTEL data plotted in Fig. 1. S. A. was supported by a Grant-in-Aid from the JSPS. E. K. acknowledges support from an Alfred P. Sloan Fellowship.

APPENDIX A: RELATION BETWEEN ANGULAR AND THREE-DIMENSIONAL POWER SPECTRUM

In this section, we derive the relation between the angular power spectrum, C_l , and the 3D power spectrum, $P_f(k)$, that we have given in Eq. (10). With the spatial Fourier transformation, Eq. (8) is rewritten as

$$\begin{aligned}
 \langle I_\gamma \rangle a_{lm} &= \int d\hat{n} \int dr \int \frac{d\mathbf{k}}{(2\pi)^3} \tilde{f}_{\mathbf{k}}(r) e^{i\mathbf{k}\cdot\mathbf{r}} W(r) Y_{lm}^*(\hat{n}) \\
 &= \int d\hat{n} \int dr \int \frac{d\mathbf{k}}{2\pi^2} \tilde{f}_{\mathbf{k}}(r) W(r) Y_{lm}^*(\hat{n}) \\
 &\quad \times \sum_{l'm'} i^{l'} j_{l'}(kr) Y_{l'm'}^*(\hat{\mathbf{k}}) Y_{l'm'}(\hat{n}) \\
 &= i^l \int dr W(r) \int \frac{d\mathbf{k}}{2\pi^2} \tilde{f}_{\mathbf{k}}(r) j_l(kr) Y_{lm}^*(\hat{\mathbf{k}}),
 \end{aligned} \tag{A1}$$

where in the second equality $e^{i\mathbf{k}\cdot\mathbf{r}}$ is expanded into the spherical harmonics and the spherical Bessel function, $j_l(kr)$, using Rayleigh's formula, and the last equality is due to the orthonormal relation of $Y_{lm}(\hat{n})$. Hence, the angular power spectrum $C_l = \langle |a_{lm}|^2 \rangle$ is expressed by

$$\begin{aligned}
 \langle I_\gamma \rangle^2 C_l &= \int dr W(r) \int dr' W(r') \frac{2}{\pi} \int d\mathbf{k} P_f(k; r, r') \\
 &\quad \times j_l(kr) j_l(kr') Y_{lm}(\hat{\mathbf{k}}) Y_{l'm'}^*(\hat{\mathbf{k}}) \\
 &= \int dr W(r) \int dr' W(r') \\
 &\quad \times \left[\frac{2}{\pi} \int k^2 dk P_f(k; r, r') j_l(kr) j_l(kr') \right],
 \end{aligned} \tag{A2}$$

where we used the definition of P_f , $\langle \tilde{f}_{\mathbf{k}}(r) \tilde{f}_{\mathbf{k}'}^*(r') \rangle = (2\pi)^3 \delta^{(3)}(\mathbf{k} - \mathbf{k}') P_f(k; r, r')$. As a final step, using the

following approximation,

$$\begin{aligned}
 &\frac{2}{\pi} \int k^2 dk P_f(k; r, r') j_l(kr) j_l(kr') \\
 &\simeq \frac{1}{r^2} P_f \left(k = \frac{l}{r}; r \right) \delta^{(1)}(r - r'),
 \end{aligned} \tag{A3}$$

which is valid if $P_f(k; r, r')$ varies relatively slowly as a function of k , we arrive at Eq. (10).

APPENDIX B: POWER SPECTRUM OF DENSITY FLUCTUATION

In this section, we summarize the power spectrum $P(k)$ of density fluctuations, δ . The detailed derivation has been given in, e.g., Refs. [41, 42, 64], to which we refer the reader. $P(k)$ includes two distinctive terms, $P(k) = P^{1h}(k) + P^{2h}(k)$, each term given by

$$P^{1h}(k) = \int_{M_{\min}}^{\infty} dM \frac{dn}{dM} \left(\frac{M}{\Omega_m \rho_c} \right)^2 |u(k|M)|^2, \tag{B1}$$

$$P^{2h}(k) = \left[\int_{M_{\min}}^{M_{\text{vir}}} dM \frac{dn}{dM} \left(\frac{M}{\Omega_m \rho_c} \right) b(M) u(k|M) \right]^2 \times P_{\text{lin}}(k), \tag{B2}$$

representing the 1-halo and 2-halo contributions, respectively. Here $u(k|M)$ is the Fourier transform of $u(r|M)$, the analytic representation for the NFW profile given by Eq. (81) of Ref. [41], $b(M)$ is the bias parameter [41], and P_{lin} is the linear power spectrum, for which we adopt the fitting formula in Ref. [53]. The values for the 1-halo and 2-halo terms as well as the linear power spectrum are shown in, e.g., Fig. 1 of Ref. [64]. The 1-halo term dominates at small spatial scales (large k).

-
- | | |
|---|---|
| <p>[1] D. N. Spergel <i>et al.</i>, <i>Astrophys. J. Suppl. Ser.</i> 148, 175 (2003).</p> <p>[2] G. Jungman, M. Kamionkowski and K. Griest, <i>Phys. Rep.</i> 267, 195 (1996).</p> <p>[3] L. Bergström, <i>Rep. Prog. Phys.</i> 63, 793 (2000).</p> <p>[4] G. Bertone, D. Hooper and J. Silk, <i>Phys. Rep.</i> 405, 279 (2005).</p> <p>[5] H. U. Bengtsson, P. Salati and J. Silk, <i>Nucl. Phys. B</i> 346, 129 (1990).</p> <p>[6] V. Berezhinsky, A. Bottino and G. Mignola, <i>Phys. Lett. B</i> 325, 136 (1994).</p> <p>[7] L. Bergström and P. Ullio, <i>Nucl. Phys. B</i> 504, 27 (1997).</p> <p>[8] L. Bergström, P. Ullio and J. H. Buckley, <i>Astropart. Phys.</i> 9, 137 (1998).</p> <p>[9] L. Bergström, J. Edsjö and C. Gunnarsson, <i>Phys. Rev. D</i> 63, 083515 (2001).</p> <p>[10] A. Cesarini, F. Fucito, A. Lionetto, A. Morselli and P. Ullio, <i>Astropart. Phys.</i> 21, 267 (2004).</p> | <p>[11] D. Hooper, I. de la Calle Perez, J. Silk, F. Ferrer and S. Sarkar, <i>J. Cosmol. Astropart. Phys.</i> 09 (2004) 002.</p> <p>[12] N. Fornengo, L. Pieri and S. Scopel, <i>Phys. Rev. D</i> 70, 103529 (2004).</p> <p>[13] D. Horns, <i>Phys. Lett. B</i> 607, 225 (2005); 611, 297(E) (2005).</p> <p>[14] P. Sreekumar <i>et al.</i>, <i>Astrophys. J.</i> 494, 523 (1998).</p> <p>[15] A. W. Strong, I. V. Moskalenko and O. Reimer, <i>Astrophys. J.</i> 613, 956 (2004).</p> <p>[16] D. E. Gruber, J. L. Matteson, L. E. Peterson and G. V. Jung, <i>Astrophys. J.</i> 520, 124 (1999).</p> <p>[17] K. Watanabe, D. H. Hartmann, M. D. Leising and L.-S. The, <i>Astrophys. J.</i> 516, 285 (1999).</p> <p>[18] S. C. Kappadath <i>et al.</i>, <i>Astron. Astrophys. Suppl. Ser.</i> 120, 619 (1996).</p> <p>[19] L. Bergström, J. Edsjö and P. Ullio, <i>Phys. Rev. Lett.</i> 87, 251301 (2001).</p> <p>[20] P. Ullio, L. Bergström, J. Edsjö and C. G. Lacey, <i>Phys.</i></p> |
|---|---|

- Rev. D **66**, 123502 (2002).
- [21] J. E. Taylor and J. Silk, Mon. Not. R. Astron. Soc. **339**, 505 (2003).
- [22] D. Elsässer and K. Mannheim, Astropart. Phys. **22**, 65 (2004).
- [23] D. Elsässer and K. Mannheim, Phys. Rev. Lett. **94**, 171302 (2005).
- [24] S. Ando, Phys. Rev. Lett. **94**, 171303 (2005).
- [25] T. Oda, T. Totani and M. Nagashima, Astrophys. J. **633**, L65 (2005).
- [26] K. Ahn and E. Komatsu, Phys. Rev. D **71**, 021303(R) (2005).
- [27] K. Ahn and E. Komatsu, Phys. Rev. D **72**, 061301(R) (2005).
- [28] G. Bertone, A. R. Zentner and J. Silk, Phys. Rev. D **72**, 103517 (2005).
- [29] D. Fargion, M. Y. Khlopov, R. V. Konoplich and R. Mignani, Phys. Rev. D **52**, 1828 (1995).
- [30] D. Fargion, R. Konoplich, M. Grossi and M. Khlopov, Astropart. Phys. **12**, 307 (2000).
- [31] K. Ahn, E. Komatsu and P. Höflich, Phys. Rev. D **71**, 121301(R) (2005).
- [32] L. E. Strigari, J. F. Beacom, T. P. Walker and P. Zhang, J. Cosmol. Astropart. Phys. **04** (2005) 017.
- [33] C. Boehm, D. Hooper, J. Silk, M. Casse and J. Paul, Phys. Rev. Lett. **92**, 101301 (2004).
- [34] J. F. Beacom, N. F. Bell and G. Bertone, Phys. Rev. Lett. **94**, 171301 (2005).
- [35] P. Jean *et al.*, Astron. Astrophys. **407**, L55 (2003).
- [36] J. Knödseder *et al.*, Astron. Astrophys. **411**, L457 (2003).
- [37] J. Beacom and H. Yuksel, astro-ph/0512411.
- [38] P. J. Zhang and J. F. Beacom, Astrophys. J. **614**, 37 (2004).
- [39] J. A. Peacock, *Cosmological Physics* (Cambridge University Press, 1999).
- [40] M. H. Salamon and F. W. Stecker, Astrophys. J. **493**, 547 (1998).
- [41] A. Cooray and R. Sheth, Phys. Rep. **372**, 1 (2002).
- [42] R. J. Scherrer and E. Bertschinger, Astrophys. J. **381**, 349 (1991).
- [43] R. K. Sheth and G. Tormen, Mon. Not. R. Astron. Soc. **308**, 119 (1999).
- [44] S. Hofmann, D. J. Schwarz and H. Stoecker, Phys. Rev. D **64**, 083507 (2001).
- [45] A. M. Green, S. Hofmann and D. J. Schwarz, Mon. Not. Roy. Astron. Soc. **353**, L23 (2004).
- [46] A. M. Green, S. Hofmann and D. J. Schwarz, JCAP **0508**, 003 (2005).
- [47] A. Loeb and M. Zaldarriaga, Phys. Rev. D **71**, 103520 (2005).
- [48] Y. Rasera, R. Teyssier, P. Sizun, B. Cordier, J. Paul, M. Casse and P. Fayet, astro-ph/0507707.
- [49] J. Diemand, B. Moore and J. Stadel, Nature **433**, 389 (2005).
- [50] V. Berezhinsky, V. Dokuchaev and Y. Eroshenko, astro-ph/0511494.
- [51] J. S. Bullock *et al.*, Mon. Not. R. Astron. Soc. **321**, 559 (2001).
- [52] V. R. Eke, J. F. Navarro and M. Steinmetz, Astrophys. J. **554**, 114 (2001).
- [53] D. J. Eisenstein and W. Hu, Astrophys. J. **511**, 5 (1997).
- [54] J. F. Navarro, C. S. Frenk and S. D. M. White, Astrophys. J. **462**, 563 (1996).
- [55] J. F. Navarro, C. S. Frenk and S. D. M. White, Astrophys. J. **490**, 493 (1997).
- [56] B. Moore, T. Quinn, F. Governato, J. Stadel and G. Lake, Mon. Not. R. Astron. Soc. **310**, 1147 (1999).
- [57] J. F. Navarro *et al.*, Mon. Not. R. Astron. Soc. **349**, 1039 (2004).
- [58] J. Diemand, B. Moore and J. Stadel, Mon. Not. R. Astron. Soc. **353**, 624 (2004).
- [59] T. Fukushige, A. Kawai and J. Makino, Astrophys. J. **606**, 625 (2004).
- [60] S. H. Hansen, Mon. Not. R. Astron. Soc. **352**, L41 (2004).
- [61] K. J. Ahn and P. R. Shapiro, Mon. Not. R. Astron. Soc. **363**, 1092 (2005).
- [62] Y. Lu, H. J. Mo, N. Katz and M. D. Weinberg, astro-ph/0508624.
- [63] Y. Ascasibar, P. Jean, C. Boehm and J. Knoedseder, astro-ph/0507142.
- [64] U. Seljak, Mon. Not. R. Astron. Soc. **318**, 203 (2000).
- [65] <http://www-glast.stanford.edu/>
- [66] D. J. Thompson *et al.*, Astrophys. J. Suppl. Ser. **86**, 629 (1993).
- [67] P. A. Milne, R. A. Kröger, J. D. Kurfess and L. S. The, New Astron. Rev. **46**, 617 (2002).
- [68] V. Schönfelder *et al.*, Astrophys. J. Suppl. Ser. **86**, 657 (1993).
- [69] L. Bergström, T. Bringmann, M. Eriksson and M. Gustafsson, hep-ph/0507229.
- [70] F. W. Stecker and M. H. Salamon, Astrophys. J. **464**, 600 (1996).
- [71] J. Chiang and R. Mukherjee, Astrophys. J. **496**, 752 (1998).
- [72] Y. C. Lin *et al.*, Astrophys. J. **401**, L61 (1992).
- [73] A. Loeb and E. Waxman, Nature **405**, 156 (2000).
- [74] T. Totani and T. Kitayama, Astrophys. J. **545**, 572 (2000).
- [75] U. Keshet, E. Waxman, A. Loeb, V. Springel and L. Hernquist, Astrophys. J. **585**, 128 (2003).
- [76] F. Miniati, Mon. Not. R. Astron. Soc. **342**, 1009 (2003).
- [77] V. Pavlidou and B. D. Fields, astro-ph/0504485.
- [78] S. Inoue, F. A. Aharonian and N. Sugiyama, Astrophys. J. **628**, L9 (2005).
- [79] W. Kawasaki and T. Totani, Astrophys. J. **576**, 679 (2002).
- [80] C. A. Scharf and R. Mukherjee, Astrophys. J. **580**, 154 (2002).
- [81] B. Moore, S. Ghigna, F. Governato, G. Lake, T. Quinn, J. Stadel and P. Tozzi, Astrophys. J. **524**, L19 (1999).
- [82] R. Aloisio, P. Blasi and A. V. Olinto, Astrophys. J. **601**, 47 (2004).
- [83] V. Berezhinsky, V. Dokuchaev and Y. Eroshenko, Phys. Rev. D **68**, 103003 (2003).
- [84] S. M. Koushiappas, A. R. Zentner and T. P. Walker, Phys. Rev. D **69**, 043501 (2004).
- [85] N. W. Evans, F. Ferrer and S. Sarkar, Phys. Rev. D **69**, 123501 (2004).
- [86] L. Pieri, E. Branchini and S. Hofmann, astro-ph/0505356.
- [87] W. de Boer, C. Sander, A. V. Gladyshev and D. I. Kazakov, astro-ph/0508617.
- [88] X. J. Bi, astro-ph/0510714.